Ocean colour observation systems for harmful algal blooms in the southern Benguela

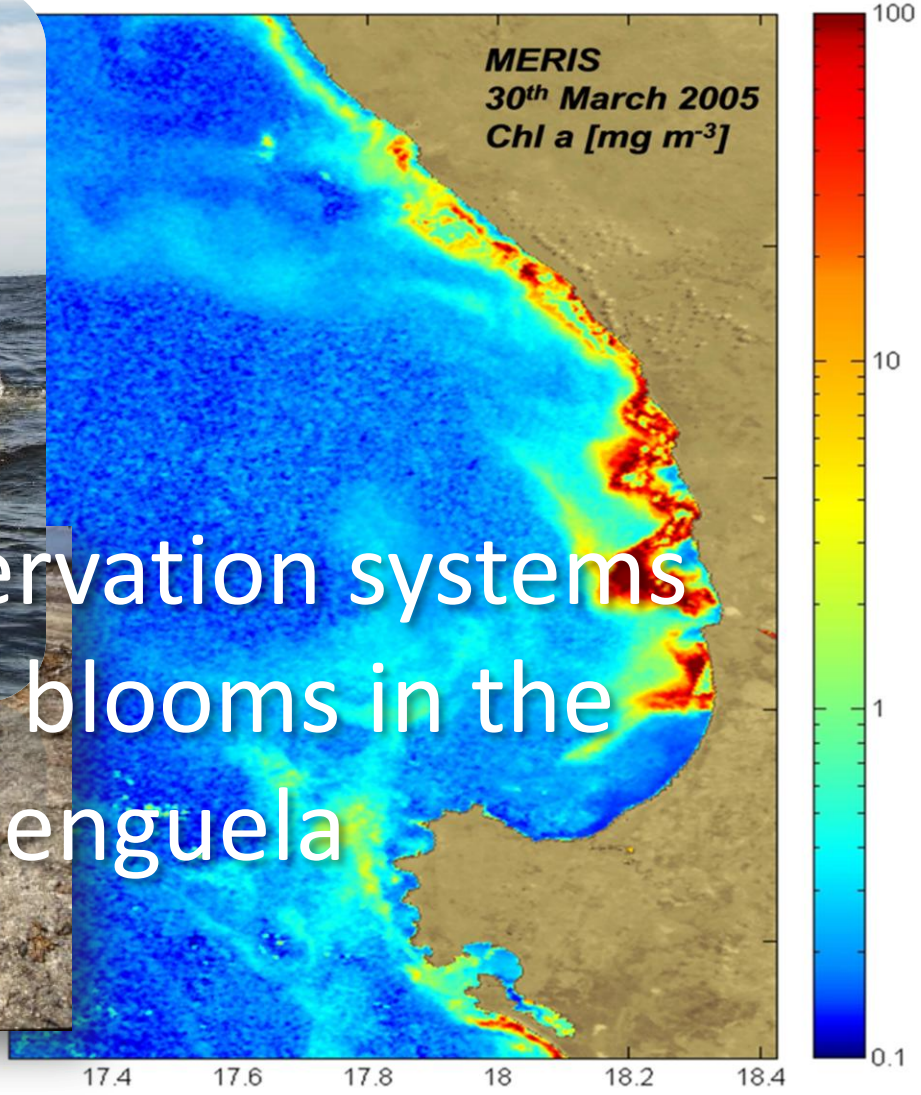

Stewart Bernard [12], Lisl Robertson[2], Mark Matthews[2]

1 Council for Scientific and Industrial Research

2 Oceanography Department, University of Cape Town

coastcolour

UNIVERSITY OF CAPE TOWN

CSIR
our future through science

Introduction & Overview

1. Overview of HABs in the Benguela
2. Broad bio-optical strategy for the Benguela
3. Algorithms for the Benguela
4. Dataset for the Benguela

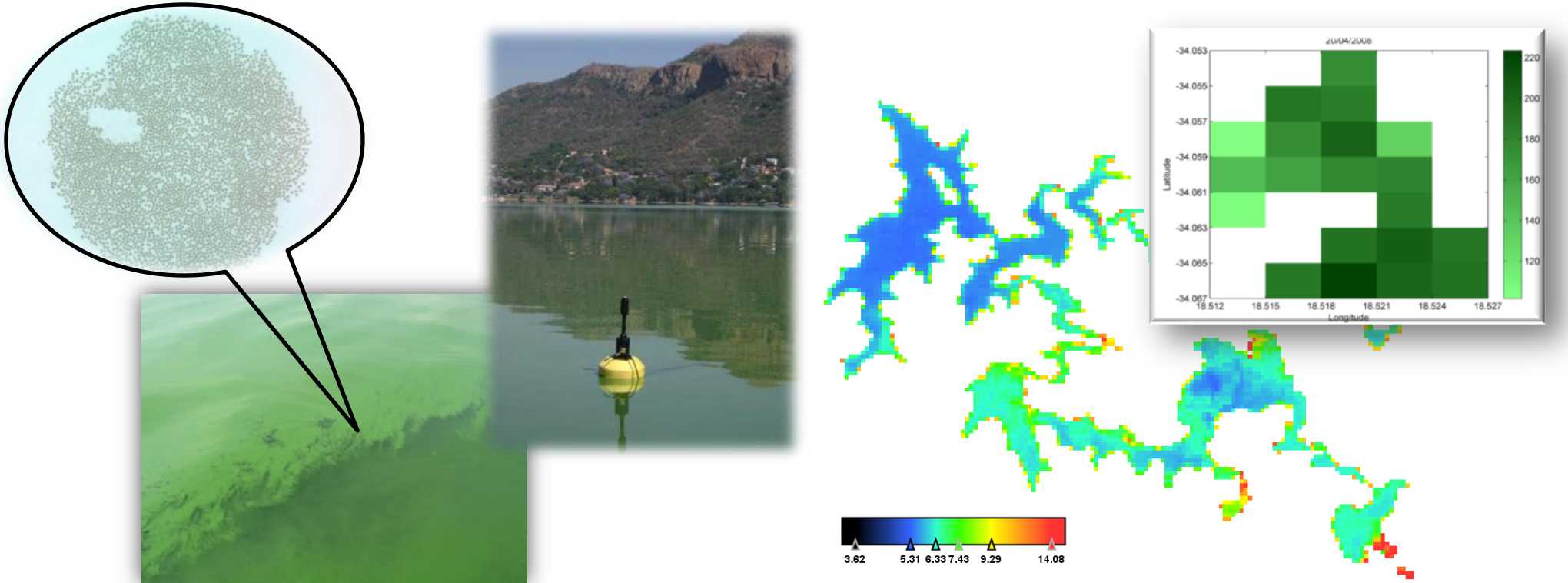

Common Types of Harmful (or not) Algal Blooms on the South African Coast

Saldanha Bay:
Heterosigma akashiwo
Aureococcus anophagefferens

Common Types of Harmful Algal Blooms on the South African Coast

South Coast:
Karenia cristata

Formation: Forcing mechanisms are not well understood, but are related to the inshore intrusion of the coastal thermal front in calm periods.

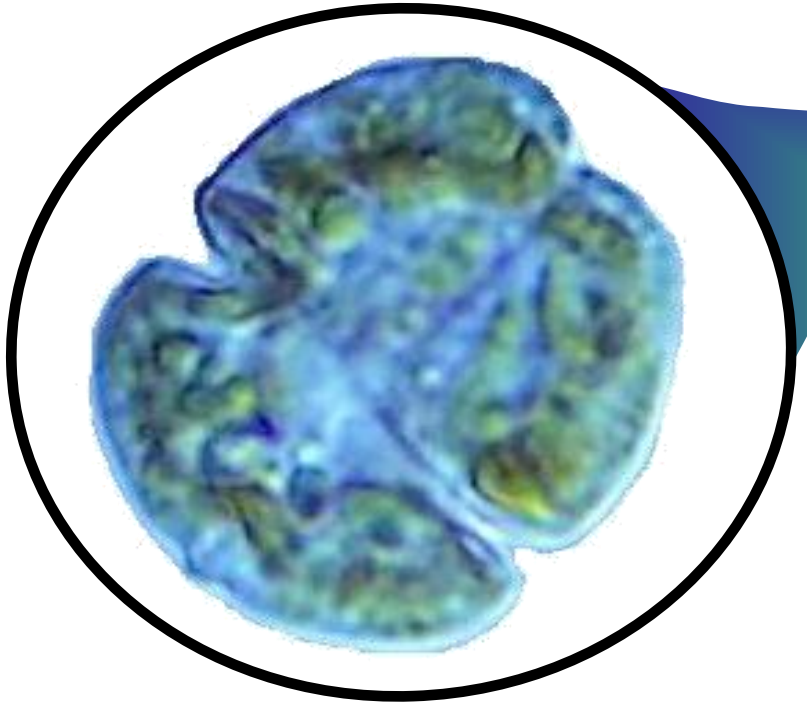

Impact: Neurotoxic Shellfish Production. Aerosol events affecting humans, wild faunal mortalities in extreme events, abalone mariculture mortalities

Common Types of Harmful Algal Blooms on the South African Coast

West Coast:
"Red Tides"

Assemblage: mixed dinoflagellate or ciliate dominated assemblages containing a variable component of PSP causing *Alexandrium catenella* and DSP causing *Dinophysis sp*., in addition to a variety of other species e.g. *Ceratium furca* and *lineatum, Gyrodinium zeta, Mesodinium rubrum, Prorocentrum sp.* Biomass can exceed 500 mg m^{-3} chl a.

Formation: Typically formed during quiescent periods in the upwelling cycle. Surface populations are advected inshore following collapse of the upwelling front, undergoing rapid growth and physical aggregation. Continued calm weather can result in shoreline retention.

Impact: Toxins enter the food chain through filter feeders and other shellfish. Collapse of high biomass blooms can lead to anoxic events resulting in mass faunal mortalities and in extreme cases, hydrogen sulphide production ("black tides").

Impacts of Harmful Algal Blooms in the Southern Benguela

West coast “red tides” are the most dramatic and well known HAB events in south African waters, due to their toxicity and the hypoxic events associated with their decay – rock lobster strandings and hydrogen sulphide related “black tides”. The worst affected regions are dynamic or physical retention zones owing to the increased likelihood of bloom collapse in these areas.

In Situ Observations

Moorings: multi-sensor lightweight coastal buoys allowing high frequency point sampling with real time data on demand, in addition to radiometric validation data. Payload of paired radiometers, other bio-optics, ADCP, thermistors [Fawcett et al 2006].

Satellite Observations

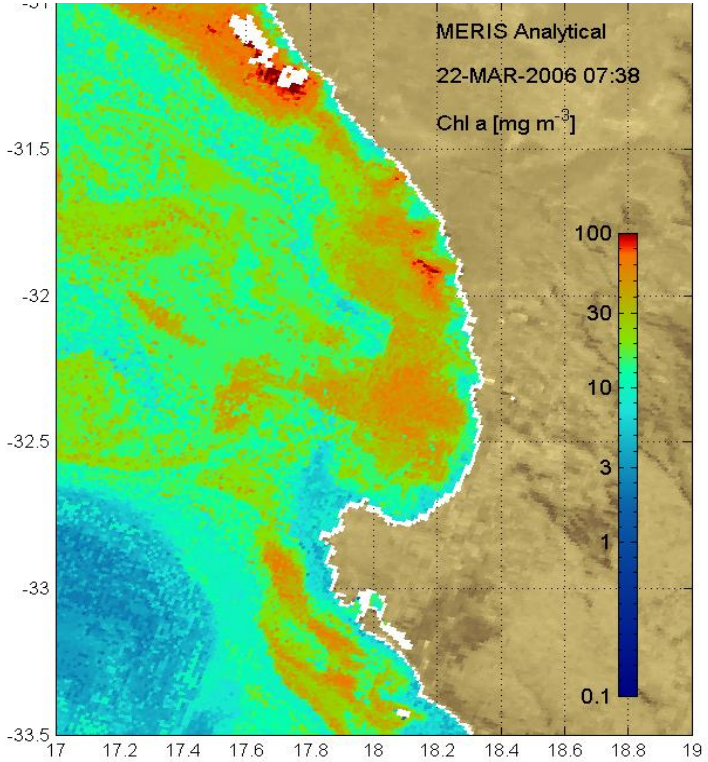

Satellites:

- MERIS RR and FR data via DDS/FTP
- MODIS data via X-band [SAC]/FTP
- AVHRR data via X-band [SAC]
- MSG2 data via EumetCast

Web based dissemination system:
www.afro-sea.org.za

Multi-scale HAB Observations: System Forcing and Assemblage Response

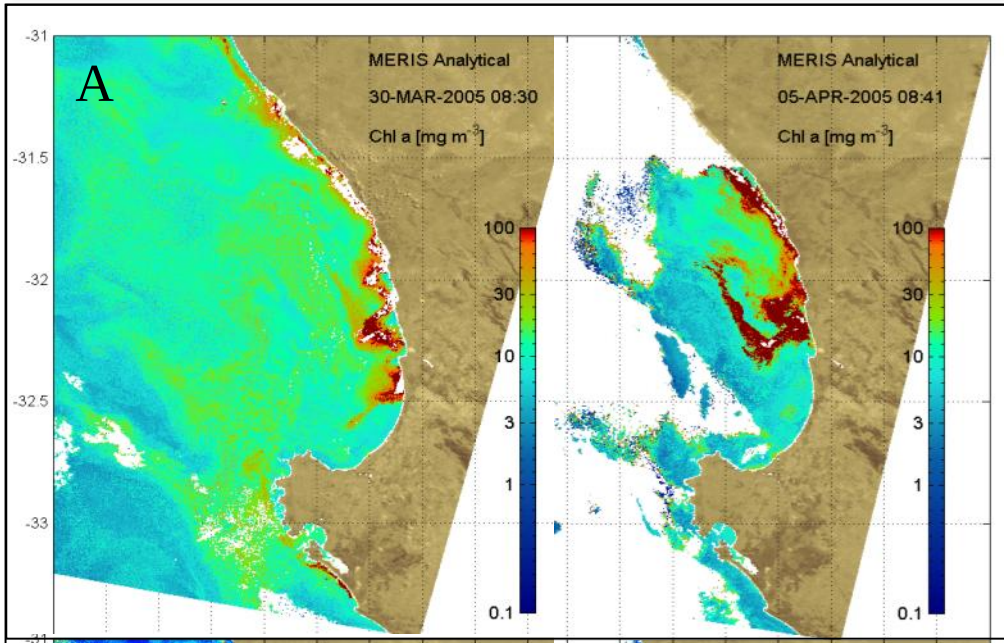

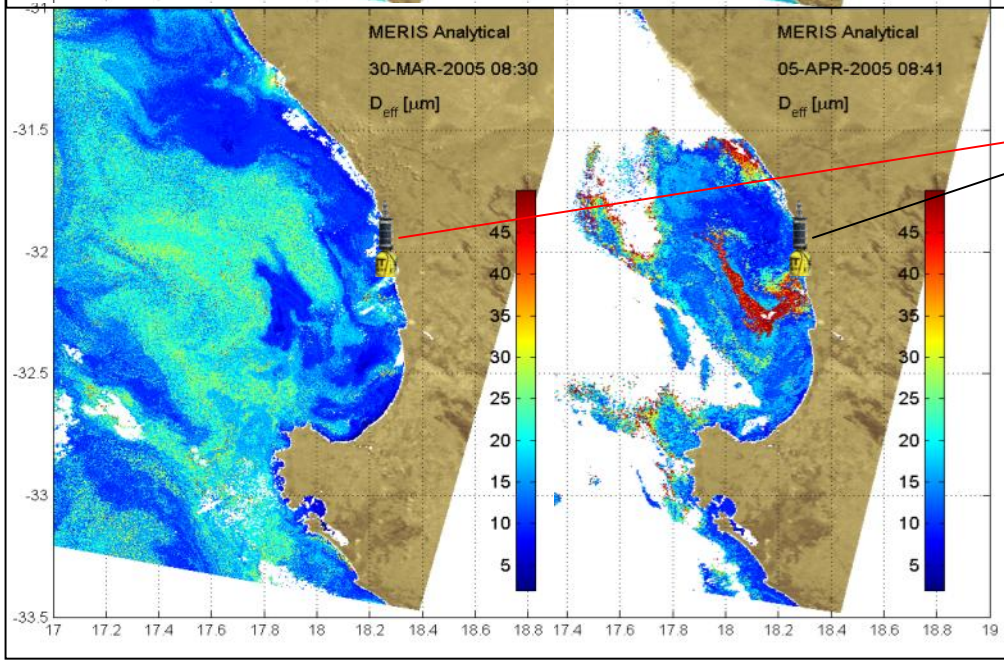

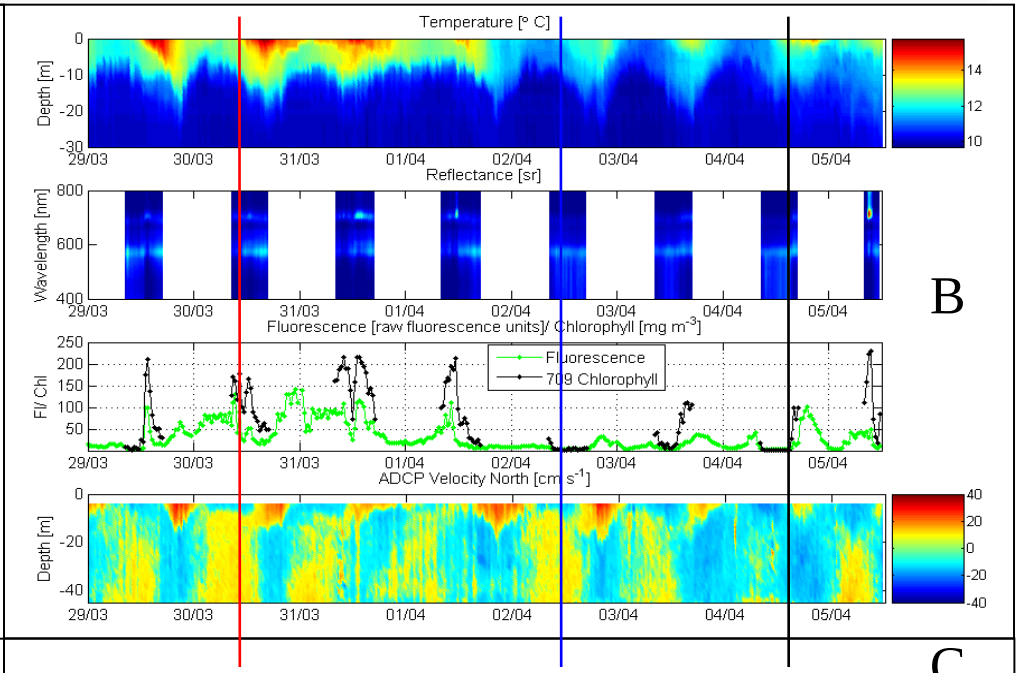

B

C

March 30 : small *Prorocentrum triestinum* dominated assemblage

April 2 : low biomass waters

April 5th : large *Ceratium furca* dominated assemblage

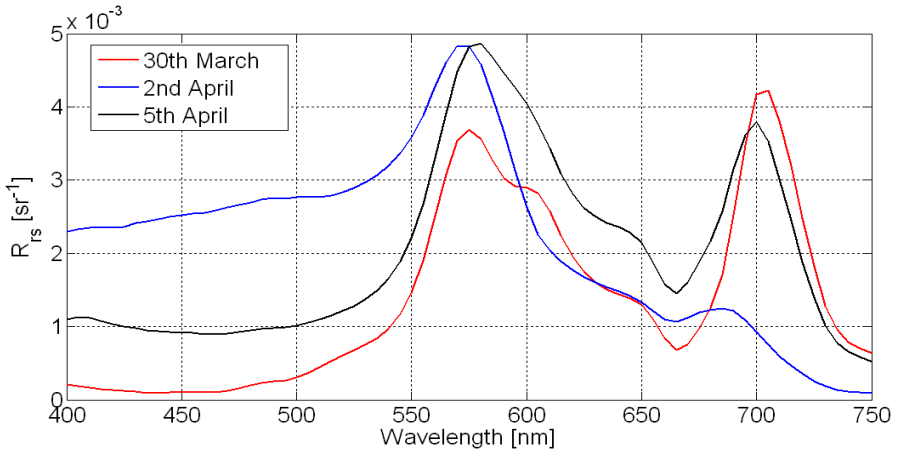

From Bio-optics to Physiology: An Allometric Approach to Phytoplankton Functionality

Demonstration of the potential to parameterise nitrogen uptake and kinetics and potential senscence onset factors using an allometric approach for typical Benguela phytoplankton assemblages

TABLE 1. Effect of cell size variation on the physical and physicochemical properties of spherical phytoplankton cells, assuming that cell composition per unit volume is independent of cell size.

Property	Effect of 10-fold increase of radius	References
Sinking speed (for cells denser than surrounding water)	Ten-fold increased speed (directly proportional to radius)	Raven (1986, 1999a,b)
Minimum energy cost of flagellar motility at a given speed	Ten-fold decrease in minimum energy cost of motility on a cell volume basis (directly proportional to radius)	Raven (1986)
Average chl *a*-specific absorption coefficient (lower value means more package effect, more intracellular self-shading)	Nonlinear decrease with increasing volume	Kirk (1994) Raven (1986, 1998, 1999a)
Average specific absorption coefficient for intracellular UV-absorbing compounds (lower value means more package effect, more intracellular self-shading)	Nonlinear decrease with increasing volume	Raven (1991, 1998, 1999a) Garcia-Pichel (1994)
Thickness of diffusion boundary layer restricting fluxes of solutes between cell surface and the bulk medium	Ten-fold increase in boundary layer thickness for radii less than ~50 μm; smaller increases in boundary layer thickness with radius increase at larger absolute radii	Raven (1986, 1998, 1999a,b) Ploug et al. (1999a,b)
Area of membrane per unit volume available for solute fluxes	Ten-fold decrease in membrane area per unit of volume	Raven (1986, 1998, 1999a,b)

Raven & Kubler 2002

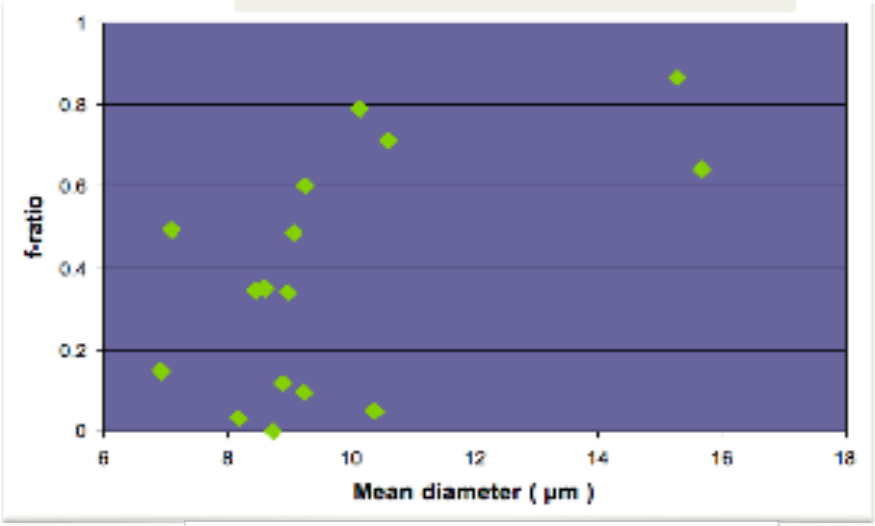

Probyn *et al.* unpublished

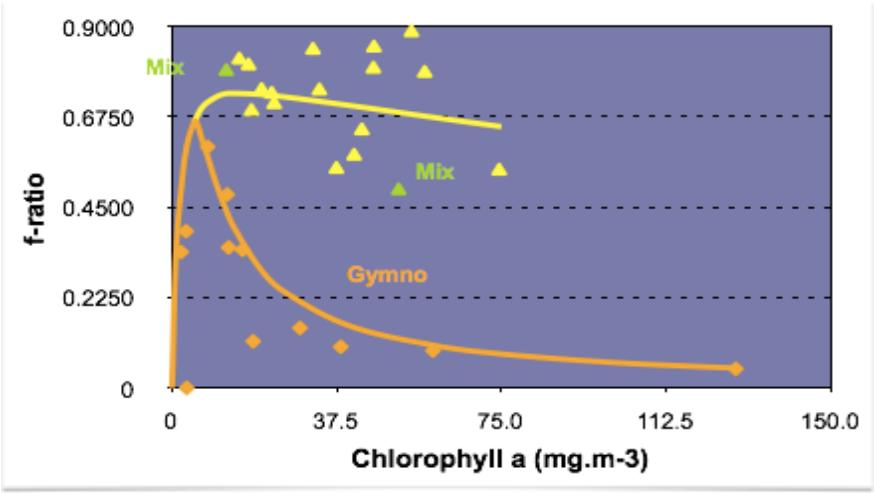

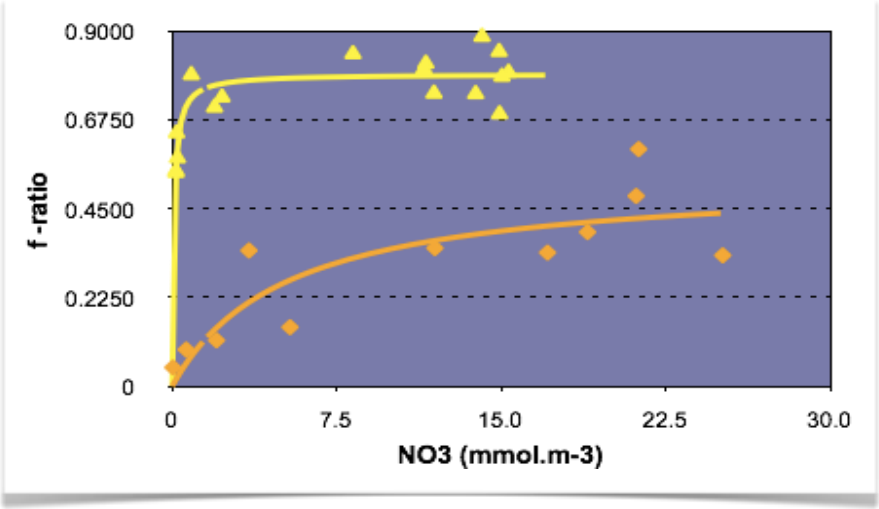

Characterising HAB Forcing & Response: Towards a Predictive Capability

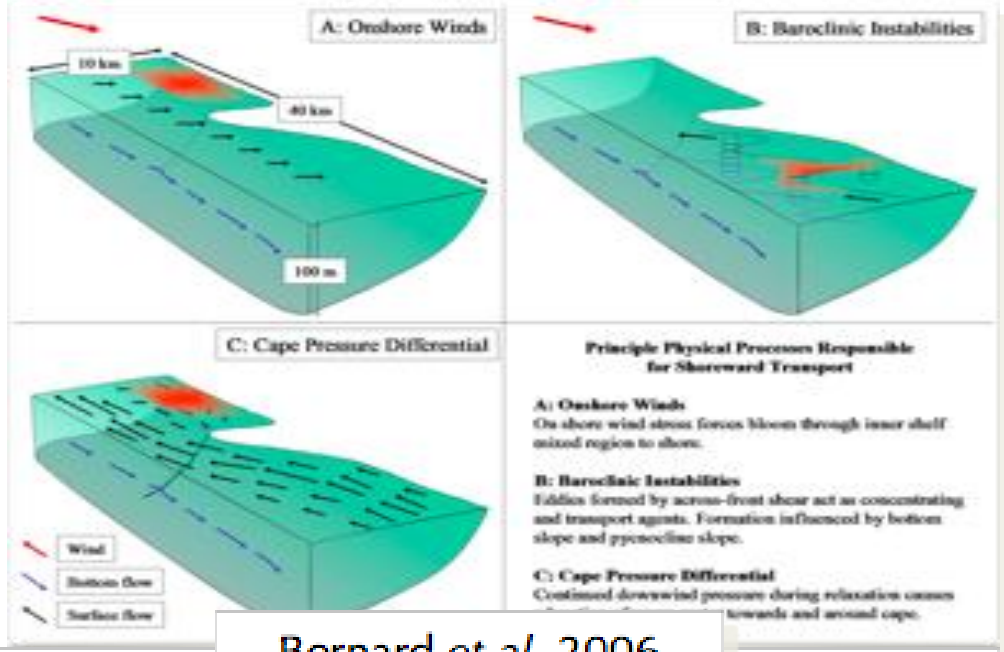

Bernard *et al.* 2006

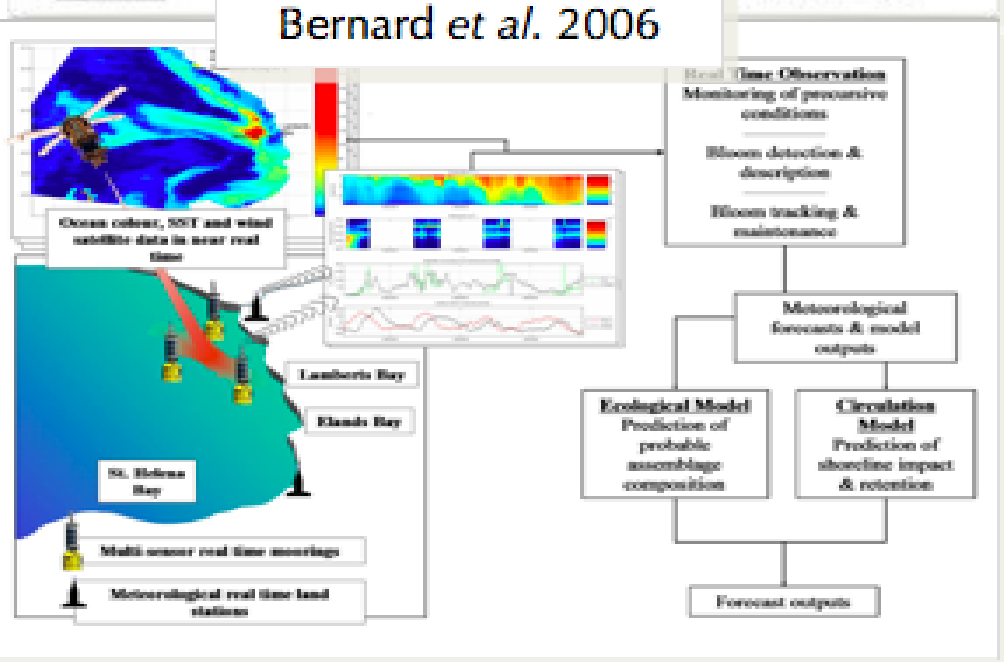

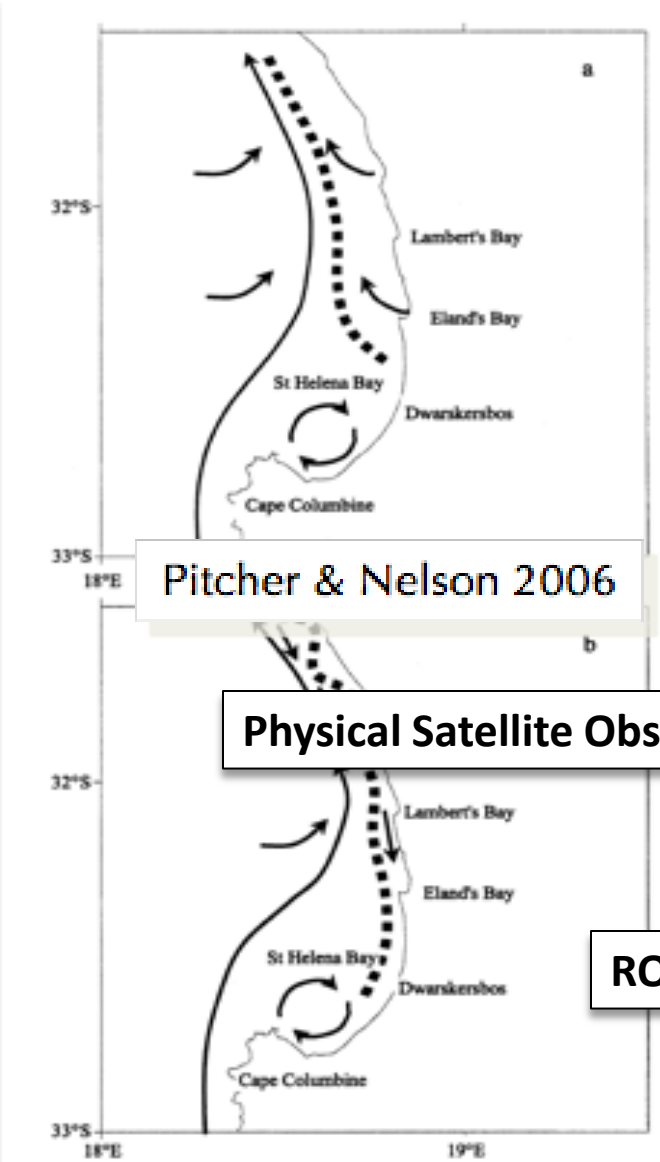

Pitcher & Nelson 2006

Physical Satellite Observations

ROMS

Fig. 15. Conceptualization of harmful bloom events in the greater St. Helena Bay region during periods of (a) upwelling and (b) relaxation or downwelling. The broken line demarcates the area of highest dinoflagellate abundance.

Analytical reflectance algorithms: size distributions of two layered spheres

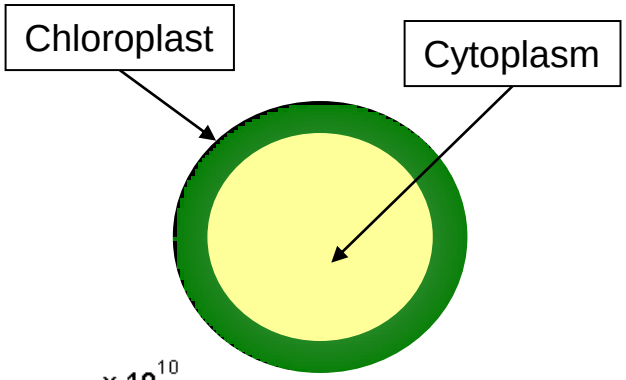

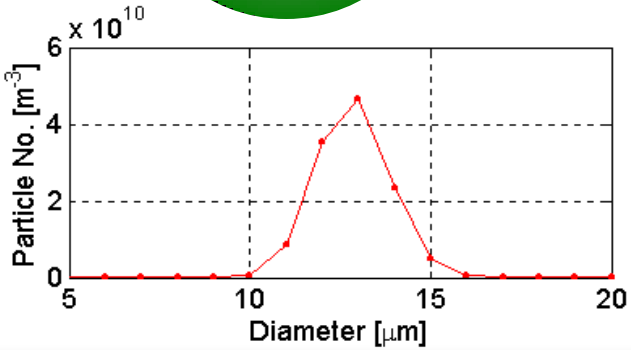

Reflectance algorithm is based on the representation of the optical properties of algal cells using two layered spheres, using standard particle size distributions to simulate polydispersed natural algal populations.

This allows algal absorption and backscattering to be manipulated with regard to average assemblage size, cellular chlorophyll concentration and accessory pigment complement

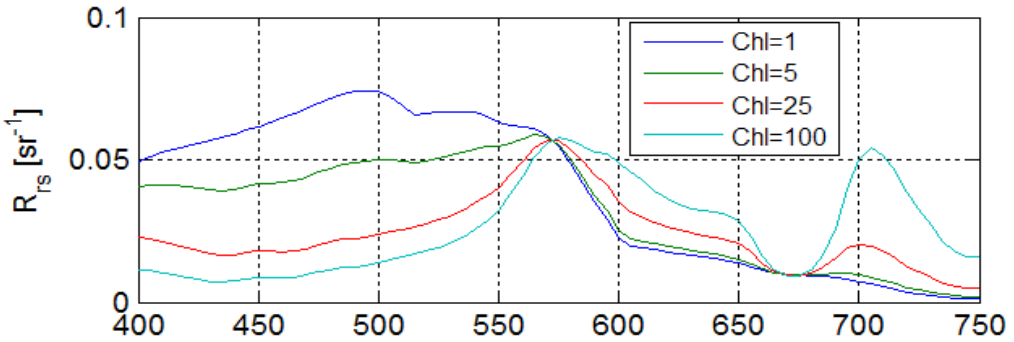

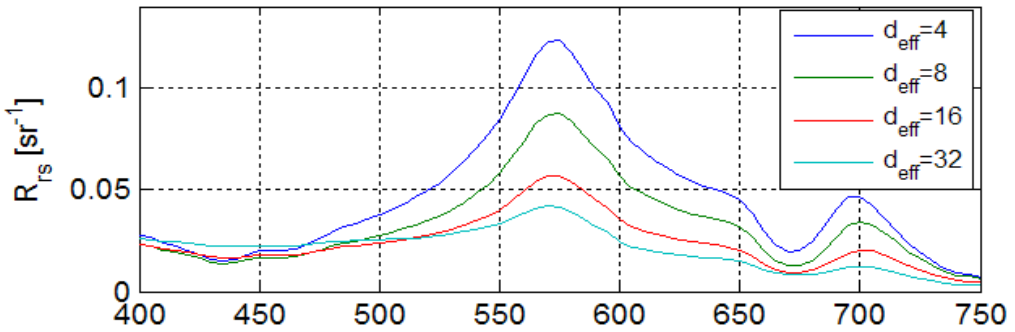

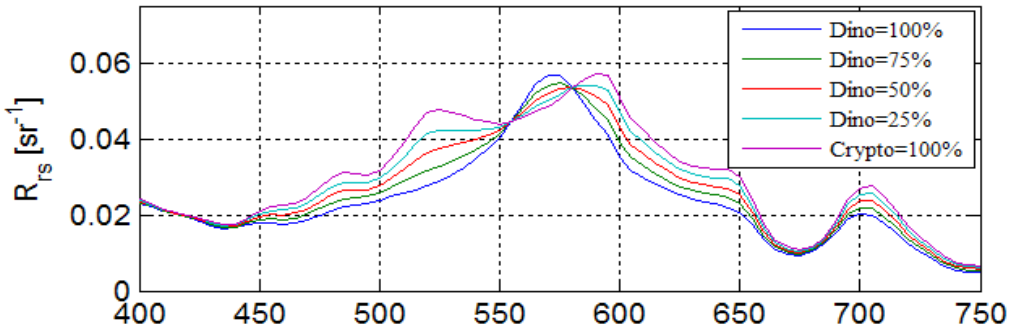

Simulated effects of changing chlorophyll concentration, effective algal diameter, and assemblage type on the reflectance spectrum

Preliminary Validation Using a Forward Reflectance Model in Bloom Conditions: Forward Modelling from a Size Distribution

Comparison of measured and simulated upwelling radiance L_u for a *Prorocentrum triestinum* bloom with cell concentrations of 1.2 *10^8 cells l^{-1}. A) Measured and simulated upwelling radiance L_u for various geometries, B) Simulated algal absorption coefficients and the absorption coefficient of pure water, C) Simulated algal backscattering coefficients and the backscattering coefficient of pure seawater, and E) Microscope derived algal size distribution.

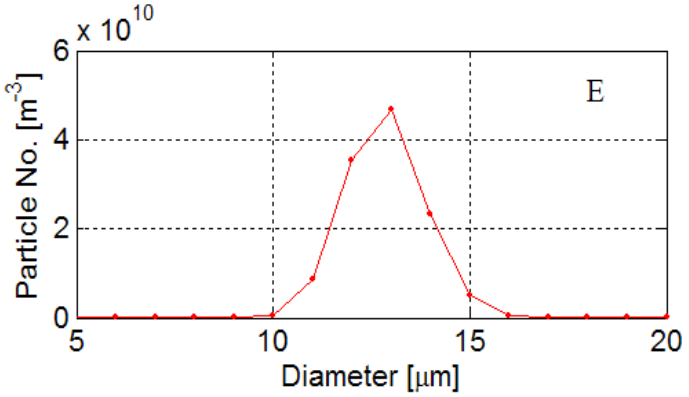

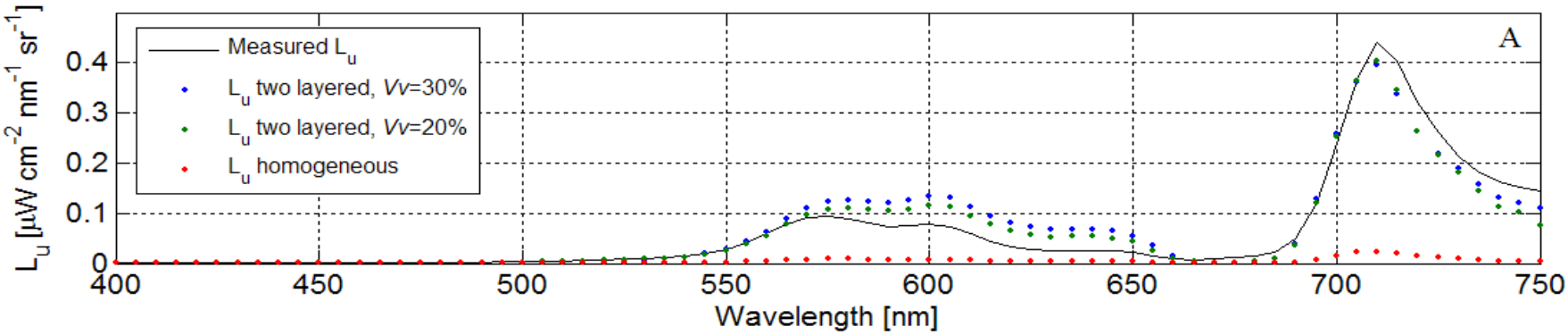

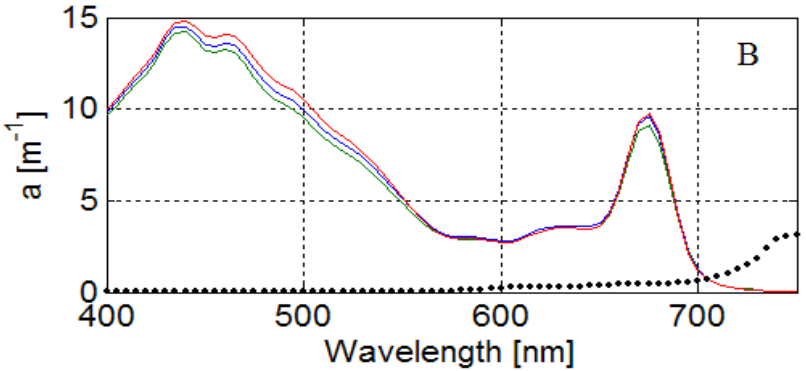

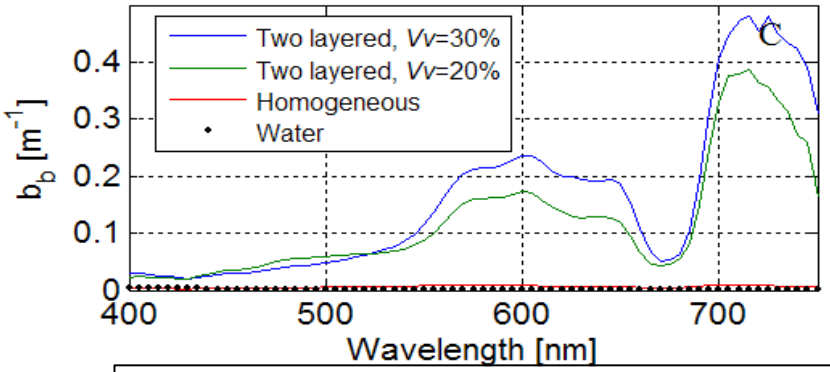

Bernard et al 2009. BioGeoSciences (Discussion)

Algorithm Performance in the Benguela: Biomass, Size and Assemblage Type

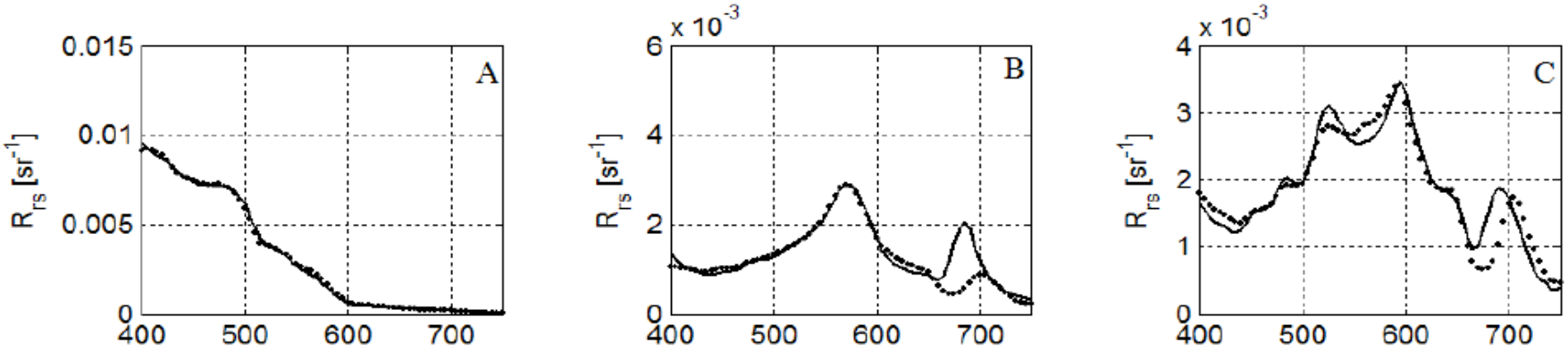

Example reflectance model matches for a range of water types. A) for low biomass flagellate dominated waters (measured Chl *a*=0.24 mg m^{-3}); B) for intermediate biomass diatom dominated waters (measured Chl *a*=20.9 mg m^{-3}); and C) for high biomass *Mesodinium rubrum*

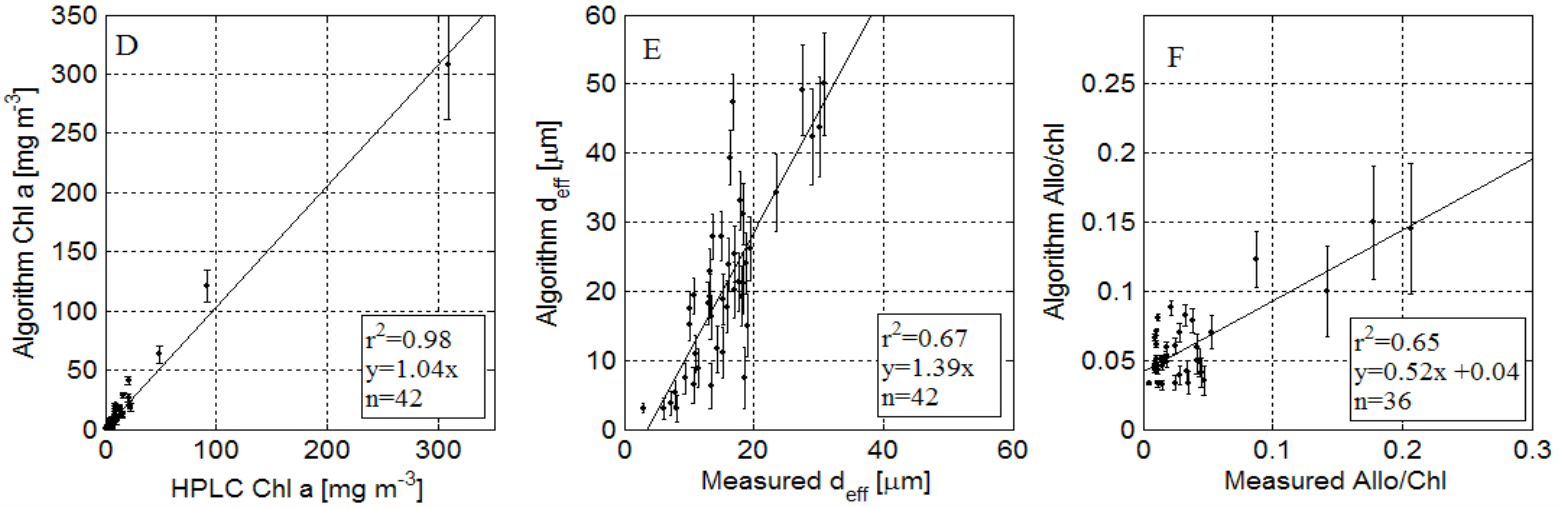

Algorithm performance, given by r^2, standard error of prediction (SEP), and linear slope values, with regard to: D) Chl *a* concentration (SEP=29%), E) effective diameter d_{eff} (SEP=47%), and F) the Allo/Chl *a* ratio: indicative here of *Mesodinium rubrum* (SEP=45%)

Simple backscattering based reflectance algorithms for high biomass application

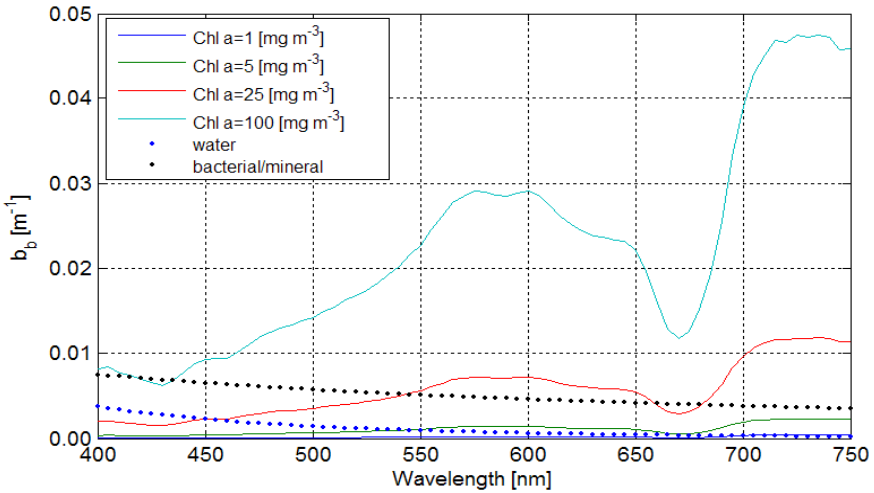

Simulated algal backscatter with increasing Chl a

Whilst analytical algorithms are very powerful, they are very expensive computationally. A simple two waveband algorithm has thus been constructed, based on the knowledge that algal backscattering offers a strong signal at red wavelengths. This algorithm has the advantage of using a strong, direct signal in high biomass waters, unlike traditional empirical ocean colour algorithms.

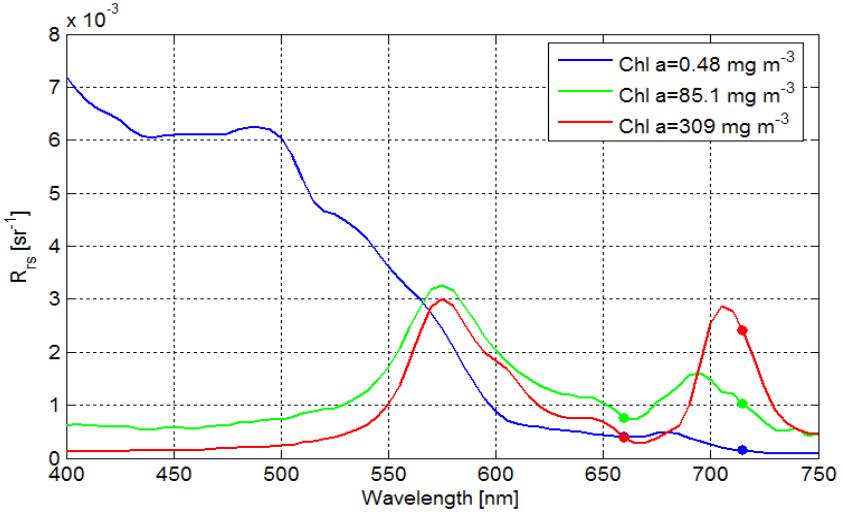

Measured reflectance with increasing Chl a

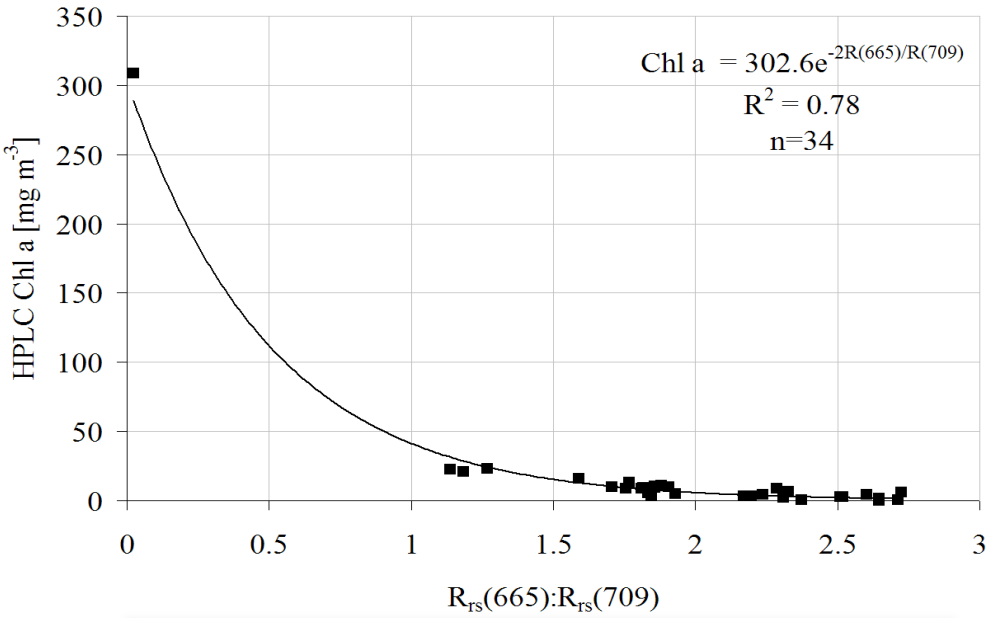

Derivation of simple two waveband algorithm

Default, Regional and Analytical Algorithms: *Alexandrium catenella* October 2002

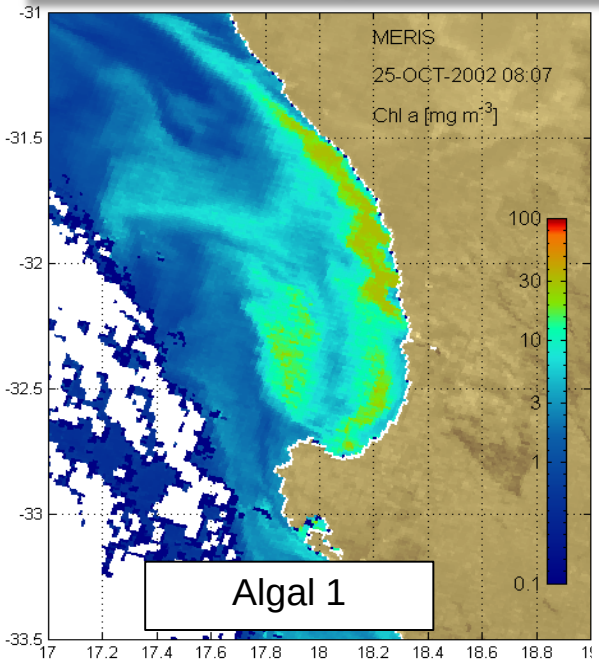

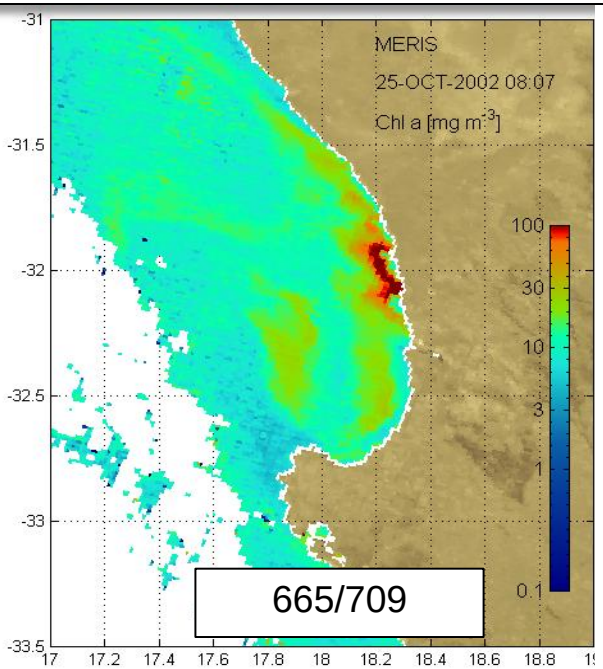

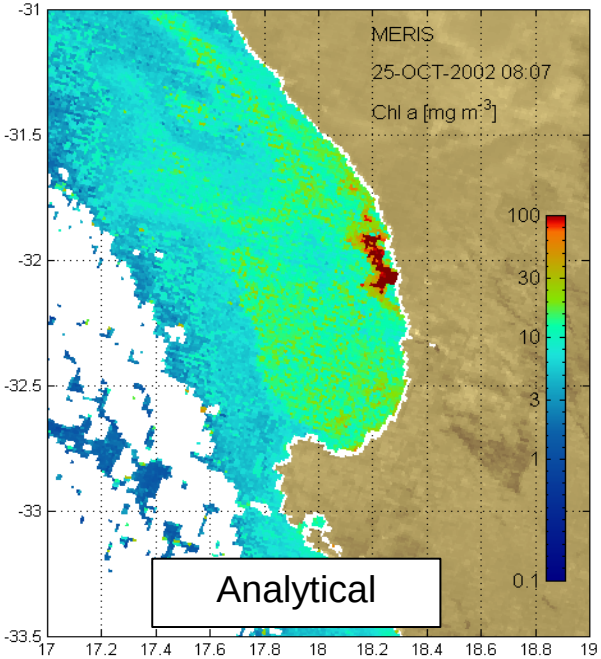

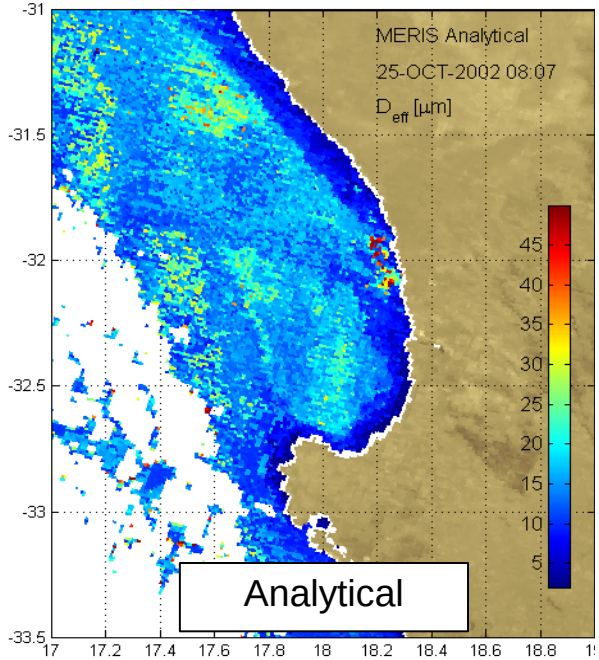

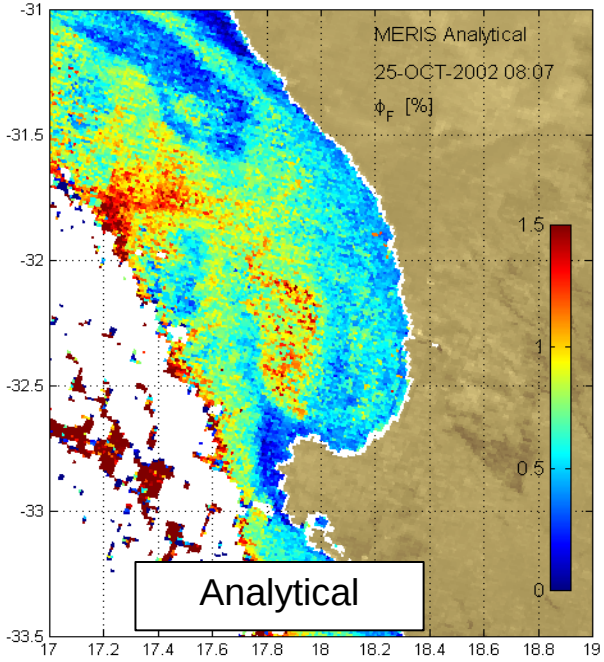

Satellite-derived images from the MERIS sensor, showing an extraordinary monospecific bloom of the PSP toxic dinoflagellate *Alexandrium catenella* in the Lambert's Bay area in October 2002. *In situ* samples showed chlorophyll a values of over 300 mg m^{-3} and cell counts of ± 10 million cells l^{-1}.

Default, Regional and Analytical Algorithms: *Prorocentrum triestinum* April 2004

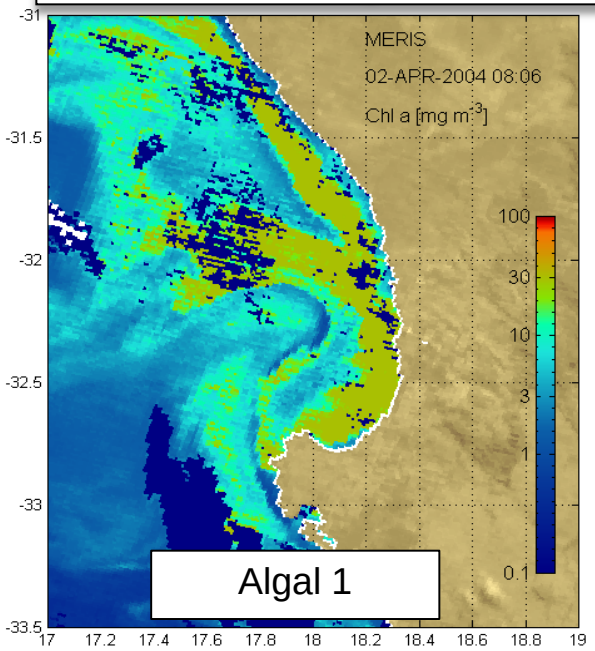

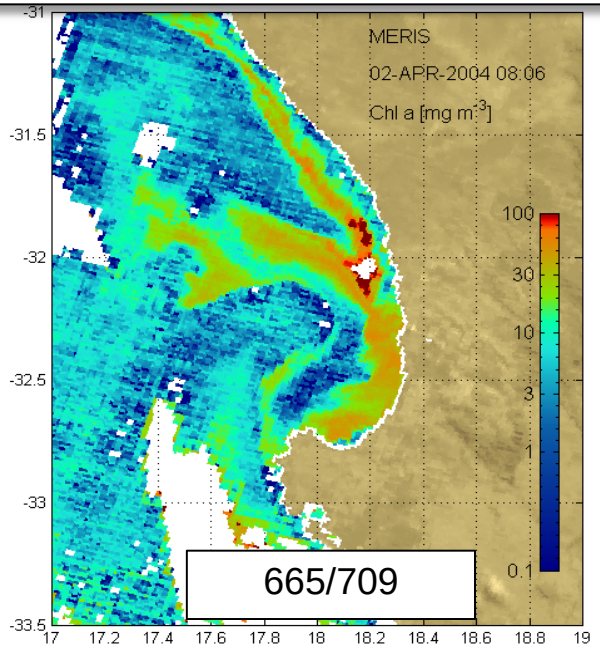

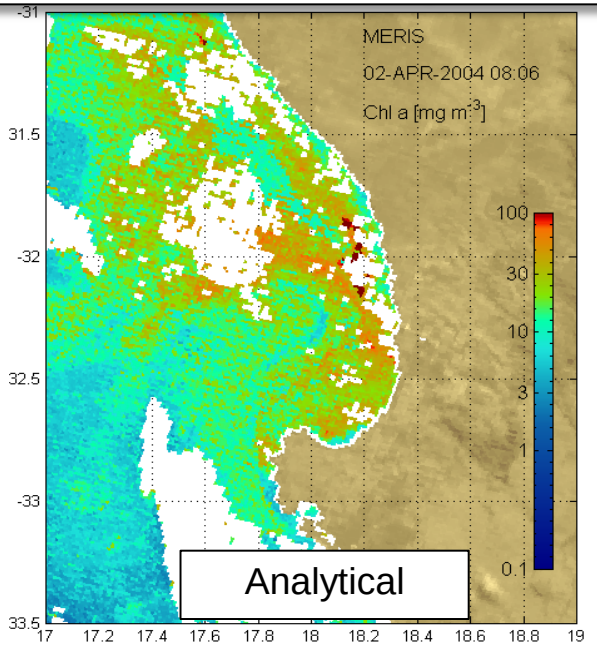

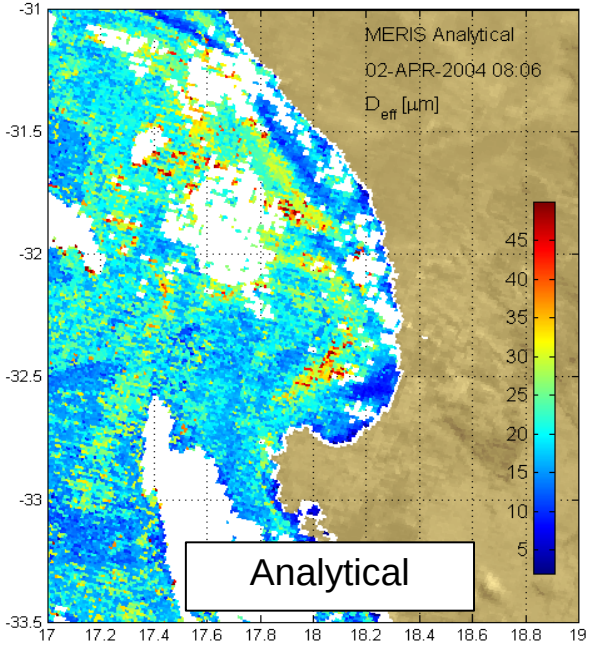

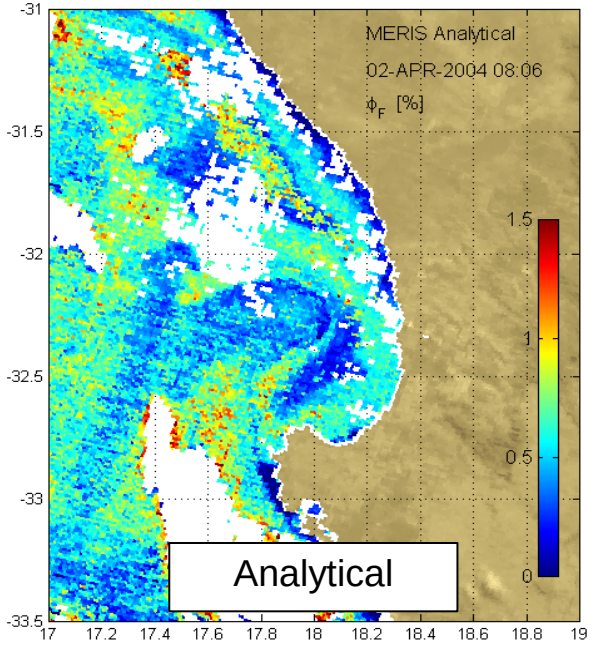

Satellite-derived images from the MERIS sensor, showing an extraordinary bloom dominated by the non- toxic dinoflagellate *Prorocentrum triestinum* in the Lambert's Bay area in April 2004. *In situ* samples showed cell counts of ± 120 million cells l^{-1}.

Default, Regional and Analytical Algorithms: *Ceratium dens* March 2009

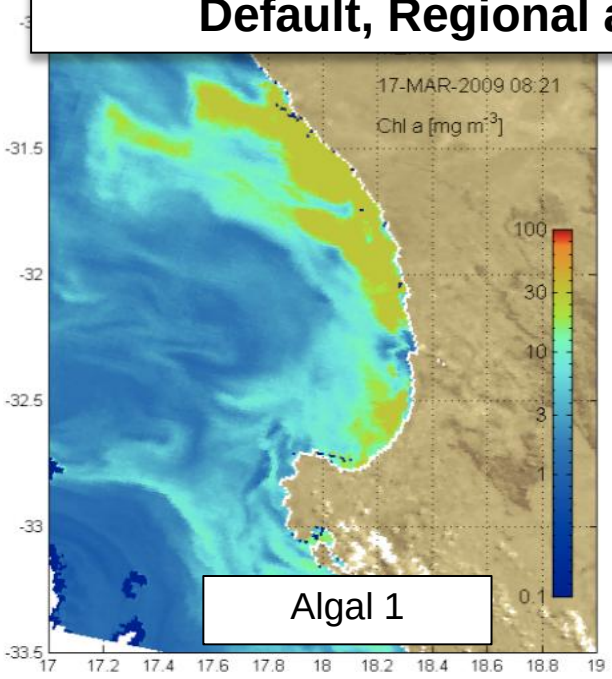

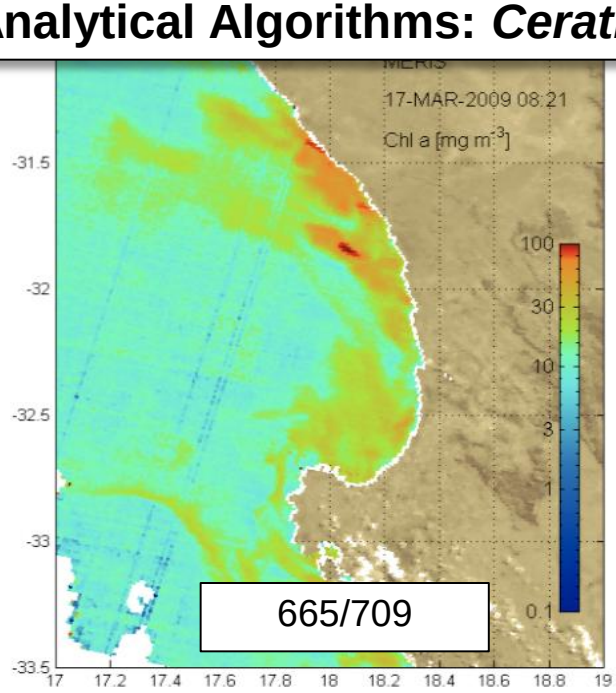

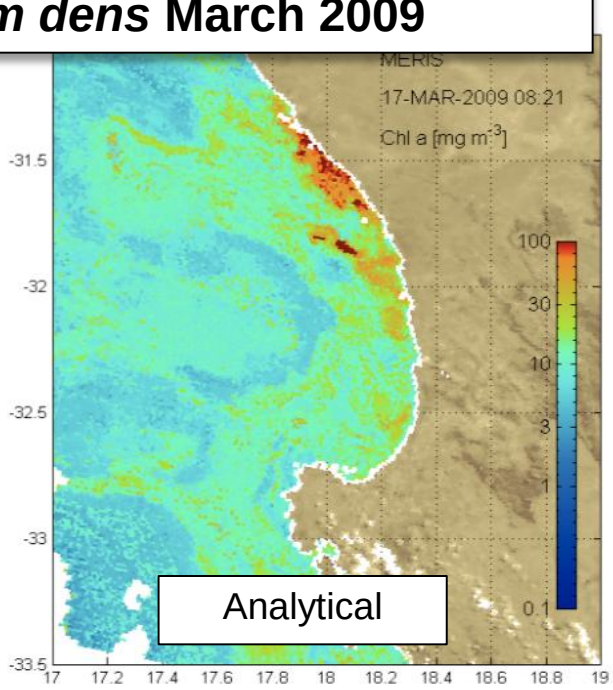

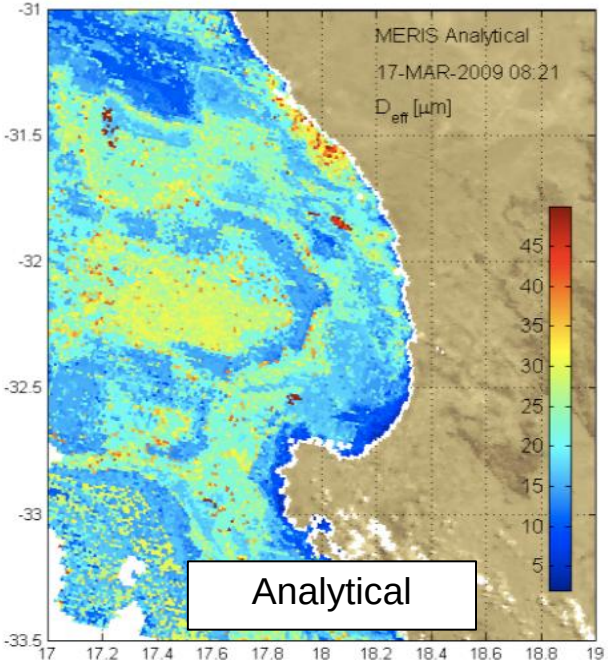

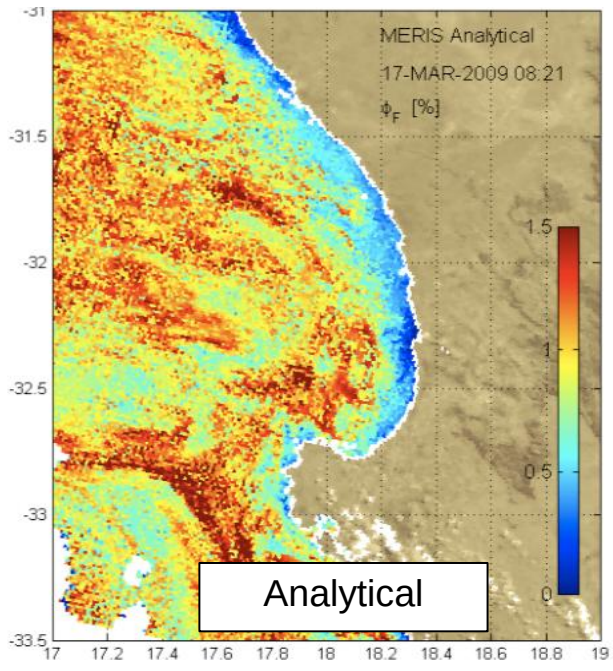

Satellite-derived images from the MERIS sensor, showing a very high biomass monospecific bloom of the non- toxic large-celled dinoflagellate *Ceratium dens* in the Lambert's Bay area in March 2005. *In situ* samples showed chlorophyll a values of over 1000 mg m^{-3} .The bloom persisted for ± 4 months

Dataset: summary

AOPs:
- Satlantic Tethered Spectral Radiometer Buoy (TSRB)
- Trios Ramses radiometers
- MERIS RR (for now...)

Biogeophysical parameters
- Chl-*a* – fluorometric or/and HPLC
- Phytoplankton assemblage and size distributions

IOPs
- a_g, a_ϕ, a_p

Atmospheric parameters
- AOT using microtops sun photometer

34 radiometric match ups from ±8 months daily data over two years

Chl estimated range: 3 to +150 mg m^{-3}

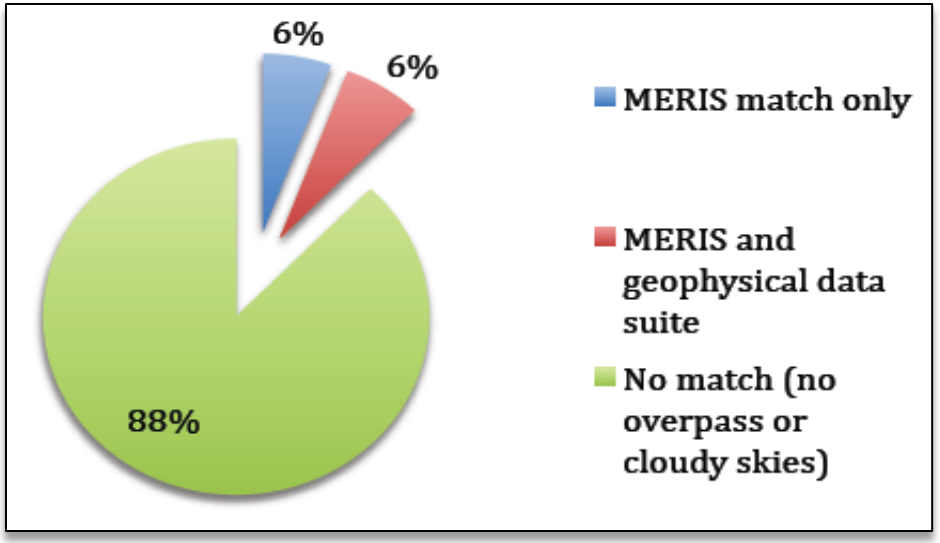

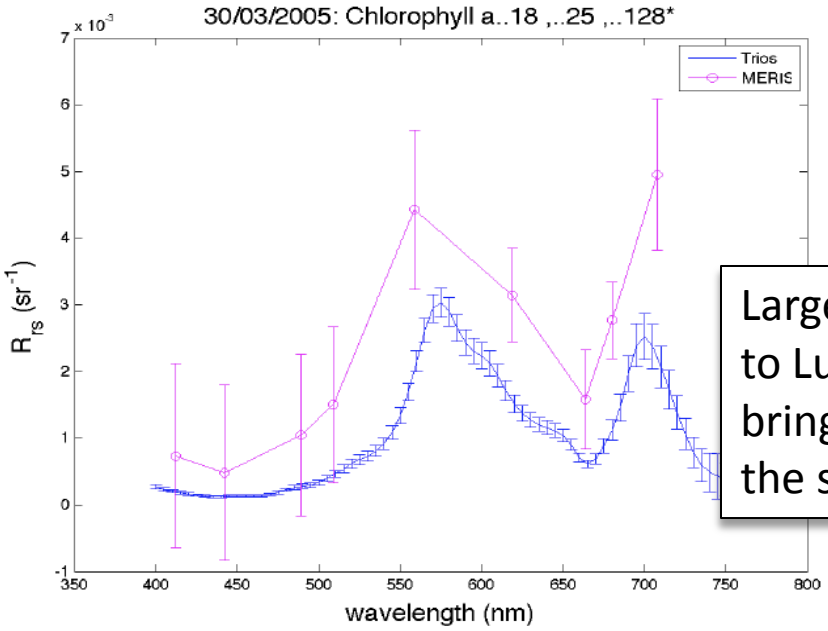

Large error introduced to Lu by using Ku to bring from 0.66 m to the surface

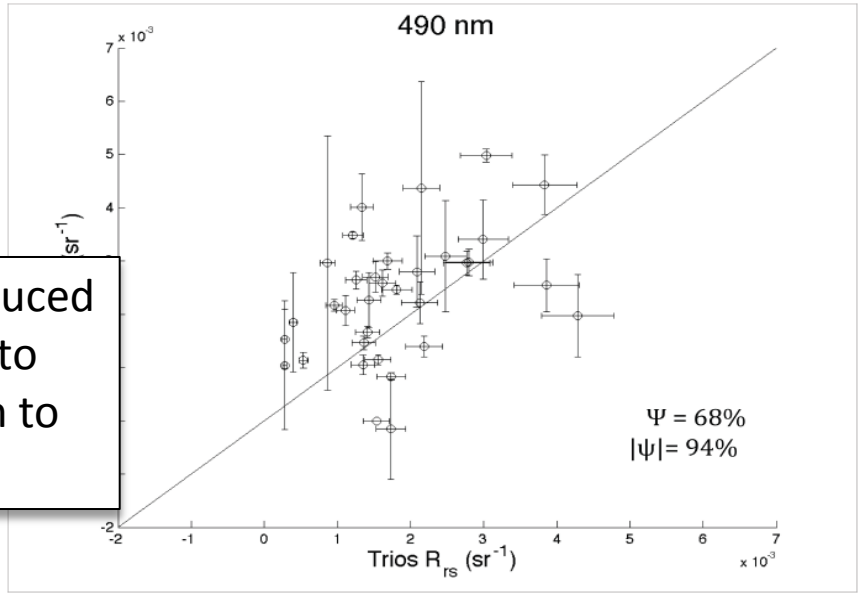

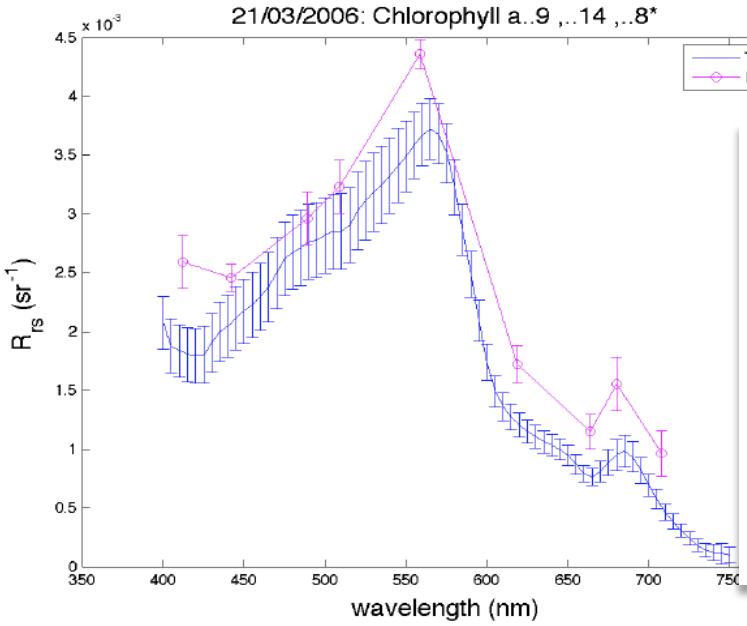

Wavelength	Coefficient
410 nm	0.10
440 nm	0.21
490 nm	0.42
510 nm	0.50
560 nm	0.71
620 nm	0.62
665 nm	0.47
680 nm	0.56
710 nm	0.79

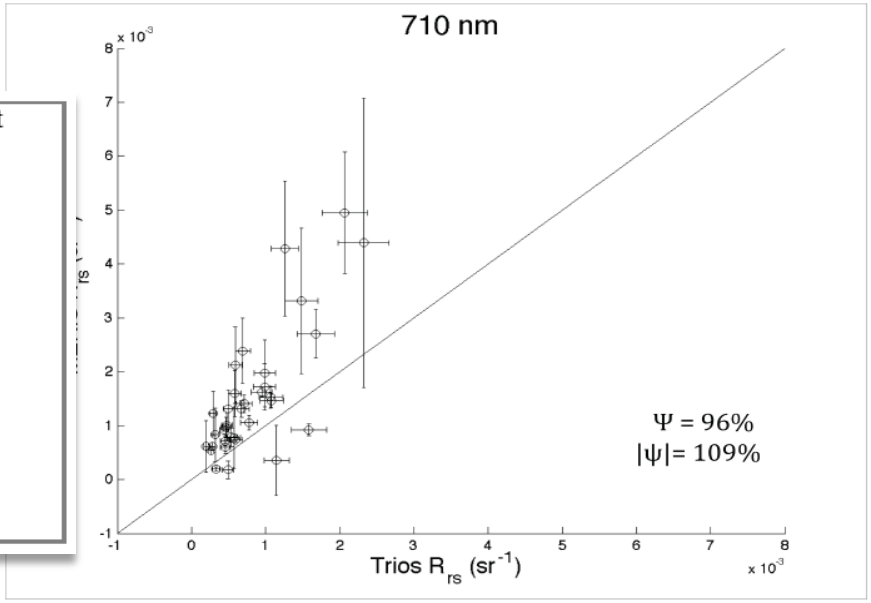

Failure of Atmospheric Correction in High Biomass Waters

665/709 Chl

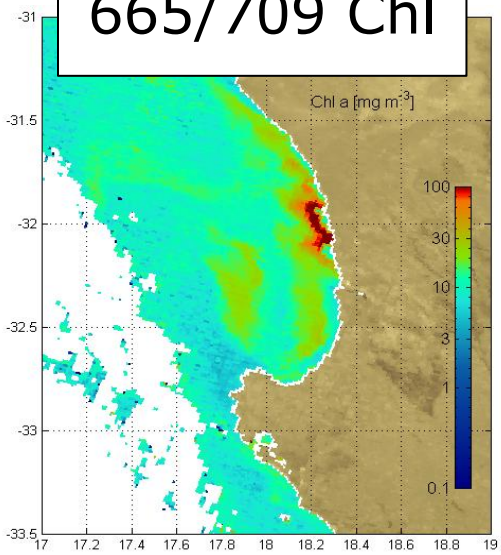

AEROSOL ANGSTROM

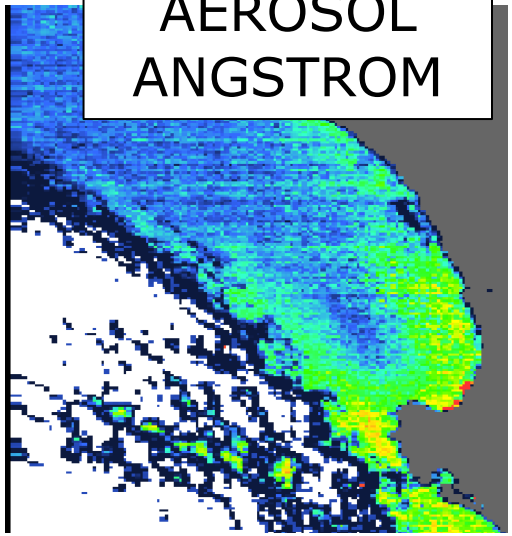

AOT 865 nm

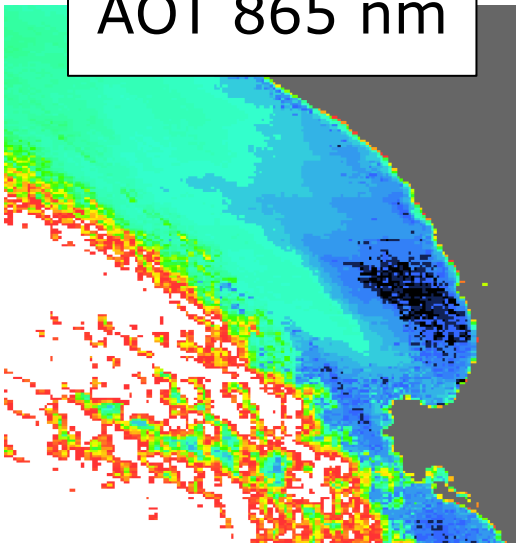

Atmospheric correction products show high spatial cohesion with in-water features, indicating likely artifacts in the atmospheric correction

$\rho_w(709)$

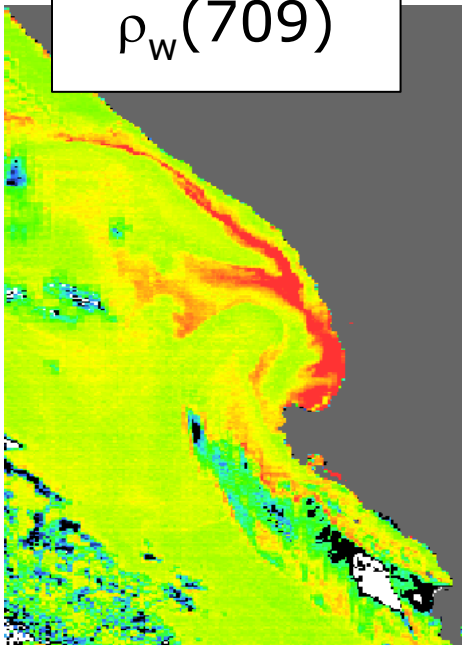

Algal 1 Chl

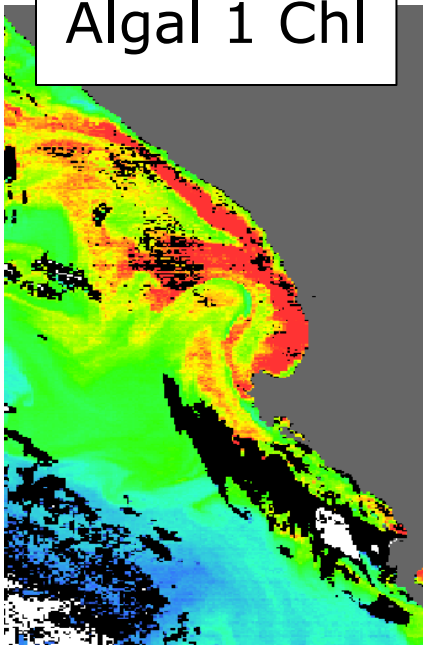

Algal 1 Chl with invalid aero products mask

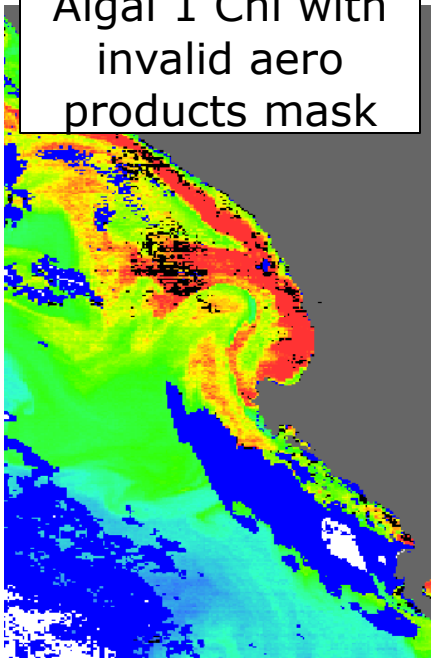

There are cases of failure of the atmospheric correction in specific instances – whether this is due to errors in identification of scattered clouds, or atmospheric features such as dust clouds is currently unclear....

End

Thanks for listening

Mark Matthews
Mark.matthews@uct.ac.za

Stewart Bernard
sbernard@csir.co.za